Density Functional Theoretical Study on Enantiomerization of 2,2′-Biphenol

Riadh Sahnoun,[†,§] Shiro Koseki,[‡] and Yuichi Fujimura*[,†]

Department of Chemistry, Graduate School of Science, Tohoku University, Sendai 980-8578, Japan, and Department of Chemistry, Graduate School of Science, Osaka Prefecture University, Osaka 599-8531, Japan

Received: September 23, 2005; In Final Form: November 20, 2005

The *S*−*R* enantiomerization processes of 2,2′-biphenol (biphenol) have been investigated using density functional theory (DFT). Five isomers for biphenol were identified: **I0**, which is the most stable isomer; **I1a** and **I1b,** which are formed by a restricted rotation of one OH group; and **I2a** and **I2b,** which are formed by a restricted rotation of the two OH groups where **a** and **b** denote cis and trans configurations, respectively. Each isomer has *R*- and *S*-enantiomers. The energies relative to the most stable isomer **I0** are 1.6, 3.3, 5.3, and 5.5 kcal mol^{-1} for **I1a**, **I1b**, **I2a,** and **I2b,** respectively. The direct enantiomerization of **I0**, in which the phenol-ring rotation is considered to be the reaction coordinate while the OH rotations are frozen, is forbidden because of the repulsion between the two OH groups. The transition states for isomerizations of **I0** to other isomers (**I1a**, **I1b**, **I2a**, or **I2b**) were calculated as well as those for the other direct enantiomerizations except for that of **I0**. From the viewpoint of the least number of the transition states and their low energy levels, the probable *S*−*R* enantiomerization of **I0** is expressed as a sequential process of isomerization: **I0,*S*** → **I1a,*S***, a direct enantiomerization induced by one of the two OH rotations, **I1a,*S*** → **I1a,*R***, and another isomerization, **I1a,*R*** → **I0,*R***, that is, **I0,*S*** → **I1a,*S*** → **I1a,*R*** → **I0,*R*** as the whole process. This process is effective in quantum control of the enantiomerization of biphenol and can be carried out by a sequence of a pump−dump IR laser-pulse scheme.

1. Introduction

Biphenols and their derivatives are important compounds in the various research fields ranging from chemistry to biology and medicine.[1−11] 2,2′-Biphenol is a fundamental biphenol owing to its ability to form inter- and intramolecular hydrogen bondings.[12,13] Another particular aspect of 2,2′-biphenol is that it has a chirality feature. Indeed, the restricted rotation around the C−C inter-ring σ-bond in 2,2′-biphenol may generate a mirror image if the hydroxy (OH) groups conserve their initial rotations, that is, without any internal rotation of the OH groups around the C−O bonds, or may lead to the formation of other isomers while maintaining OH initial rotational angles. This kind of chirality, known as axial chirality, is of special importance if the rotational barrier is large enough to prevent a rapid interconversion so that the conformational isomers, also known as "atropisomers", can be isolated and studied separately.[14]

Chiral molecules are of particular importance since they can be used as probe molecules for investigating some of the fundamental chemical and biological processes. Recently, many studies have addressed the issue of quantum control of molecular chirality because of its important chemical processes and also because of the progress made in laser science and technology.[15−19] In this regard, several methods for quantum control of enantiomerization, which is a conversion of one enantiomer to another, of chiral compounds have been proposed.[20−23]

In a recent work, we investigated the 1,1′-bi-2-naphthol (binaphthol) molecule, and we addressed the question of possible direct enantiomerization, by the rotation around the C−C inter-ring bond, of the most stable isomer.[24] In this work, we aim to elucidate all possible enantiomerization or isomerization processes starting by identifying all possible biphenol isomers. So far, three isomers have been detected by various experimental techniques and confirmed by theoretical methods. To the best of our knowledge, there has been no theoretical study on the enantiomerization mechanism of 2,2′-biphenol nor any study on the number of isomers that it may have. We have, therefore, undertaken a systematic investigation on this issue.

For this purpose, we present in this paper the results of a molecular orbital theoretical study on the enantiomerization processes of 2,2′-biphenol (hereafter called simply biphenol). As in our previous studies where two molecules, namely difluorobenzophenanthrene and binaphthol were considered as targets for quantum control of enantiomers,[25,26] the results of the present work equips us with the fundamental data for an effective scenario for biphenol's quantum control.[27] We show the probable *S*−*R* enantiomerization path between the most stable enantiomers and explain the mechanism of the enantiomerization in terms of both the C−C inter-ring (phenol/phenol) rotation and the OH rotations around the C−O bonds.

This paper is organized as follows. In the next section, we briefly describe the method of calculations. In the next section, we first show the stabilities of the isomers of biphenol and discuss the origin of the conformational preference in their structures. Next, we present possible enantiomerization pathways and the most favorable *S*−*R* enantiomerization pathway of the most stable isomer. Finally, we discuss the applicability of quantum control to *S*−*R* enantiomerization of biphenol.

2. Computational Details

Geometry optimizations were carried out at the B3LYP level of the density functional theory, which consists of the hybrid

* Corresponding author. Tel. and Fax: 81-22-795-7715. E-mail: fujimurayuichi@mail.tains.tohoku.ac.jp.
† Tohoku University.
‡ Osaka Prefecture University.
§ E-mail:sahnoun@mcl.chem.tohoku.ac.jp.

10.1021/jp0554137 CCC: $33.50
Published on Web 01/27/2006

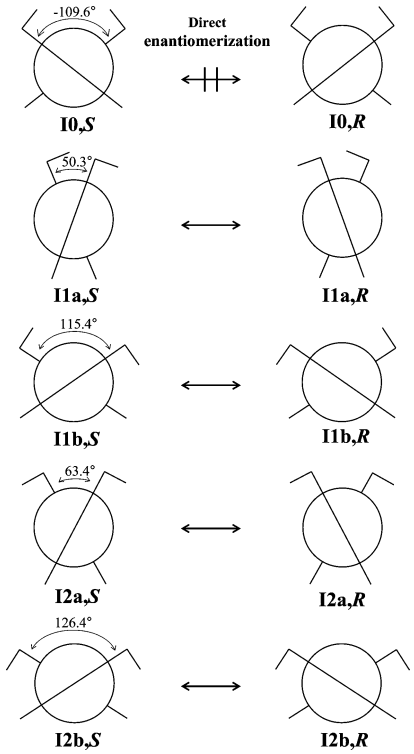

Figure 1. Five isomers of 2,2′-biphenol, **I0**, **I1a**, **I1b**, **I2a**, and **I2b** and their respective enantiomers. **I0** denotes the most stable isomer. The phenol group is graphically abbreviated by a bar having a short stick that represents the hydroxy (OH) group. **I1a** and **I1b** denote isomers formed by a rotation of one of the two OH groups. **I2a** and **I2b** denote isomers formed by rotation of both OH groups. The numerical value denotes the calculated dihedral angle between two phenol groups of each enantiomer. The direct enantiomerization between **I0,*S*** and **I0,*R*** is forbidden, while the other direct enantiomerizations are allowed.

Becke+Hartree−Fock exchange and the Lee−Yang−Parr correlation functional with nonlocal corrections.[28] We used the 6-31+G(d,p) basis set as implemented in the Gaussian suites program. Where appropriate, symmetry of isomers was considered. However, for the sake of consistency, all of the equilibrium and transition state structures determined were optimized without any symmetry restriction. All of the structures were identified by the number of imaginary frequencies calculated from the analytical Hessian matrix. The reaction coordinates were followed from each transition state to the reactant and product on the potential energy curve by the intrinsic reaction coordinate (IRC) technique.[29] For the most favorable path, thermochemical parameters—enthalpy, entropy, and Gibbs free energy—were calculated at the B3LYP/6-31+G-(d,p) level using a scaling factor 0.9614[30] for the calculated vibrational frequencies at the temperature of 298.15 K and pressure of 1 atm.

For the most favorable path, single-point energy calculations at the optimized B3LYP/6-31+G(d,p) structures have been carried out at the MP2(fc)/6-31+G(d,p) level of theory for comparative purposes.[31]

All calculations were carried out using the Gaussian 98[32] and Gaussian 03[33] suites of the program.

3. Results and Discussion

3a. Isomers of 2,2′-Biphenol. Figure 1 shows five isomers designated **I0**, **I1a**, **I1b**, **I2a**, and **I2b**, which were found by using the DFT theoretical method.[34] Their relative energies with respect to the most stable isomer **I0** are 1.6 kcal mol^{-1} for **I1a**, 3.2 kcal mol^{-1} for **I1b**, 5.3 kcal mol^{-1} for **I2a**, and 5.5 kcal mol^{-1} for **I2b**.

Each of these isomers has its enantiomer counterparts, *S*- and *R*-forms. Here, **I0** denotes the most stable isomer. **I1a** (**I1b**) and **I2a** (**I2b**) denote the isomers that are formed by a restricted rotation of one (**1**) of the two OH groups and that of both (**2**) OH groups, respectively; **a** and **b** denote cis and trans configurations, respectively. In addition to the three cis isomers **I0**, **I1a,** and **I2a** that should, in principle, be possible structures from the viewpoint of interactions between the two OH groups, another two isomers, **I1b** and **I2b,** were found to be stable ones. As can be seen from Figure 2, these latter two isomers (**I1b** and **I2b**) are the result of rotation around the C−C inter-ring σ-bond of the two former isomers (**I1a** and **I2a**), where the two OH groups are away from each other.

Figure 2 shows the geometrical structures of the five isomers, which were calculated at the B3LYP/6-31+G(d,p) level. The geometrical structure for isomer **I0** compares reasonably well with those calculated by Ottaviani et al.,[35] within 0.003 Å and 0.2° as the maximum deviations in bond lengths and angles, respectively. The ring−ring dihedral angle of 109.6° lies between the DFT value of 107° and the experimental value of 112.7°, which were determined by using millimeter wave absorption free jet spectroscopy.[35] The dihedral angle is significantly different from the calculated semiempirical value of 55° reported by Lucarini and co-workers using the AM1 method.[36]

The two aromatic rings in **I1a** and those in **I2a** bend toward each other, forming rotational dihedral angles of 50.3° and 63.4°, respectively. These angles are half of that of **I0**. In **I1b** and **I2b**, the two aromatic rings are separated from each other by 115.4° and 126.4°, respectively, which are somehow larger than that in **I0**.

The calculated dihedral angles for **I1a** and those for **I2a** compare reasonably well with those determined by crystal structure experiments. Indeed, the ring−ring dihedral angle was evaluated to be 48.4° in **I1a**,[37] in good agreement with the calculated angle of 50.3°. Overall, the geometrical parameters determined experimentally are within 0.03 Å for the bond lengths but less than 1° for the bond angles, indicating good agreement with our DFT results.

For **I2a**, no published results are available for the isolated isomer. However, the crystal structure of the monohydrate complex has been reported,[13] and it would be worth comparing our calculated structure with the crystal structure. At first, it should be noted that the monohydrate biphenol does not exhibit the expected C_2 symmetry as was the case in our calculation, due to the presence of the intermolecular hydrogen bond. Nevertheless, comparison between the monohydrate biphenol geometrical parameters and our calculated ones shows relatively good agreement in terms of bond lengths and angles. Regarding the dihedral angle between the two aromatic rings, our calculated value of 63.4° is slightly smaller than that in the monohydrate one, 67.6°.[13] This deviation is attributed to the effects of the intermolecular hydrogen bond between the water molecule and one of the two oxygen atoms in the monohydrate form. Second, while narrowing of the rotational dihedral angle in **I1a** is clearly attributed to the formation of a hydrogen bond between the two OH groups, the electrostatic repulsion between the two oxygen atoms in the case of the **I2a** isomer somehow widens its rotational dihedral angle by about 13.1°, compared to that in **I1a**.

For **I0**, **I1b**, and **I2b**, the rotational dihedral angle was even much larger. One explanation for widening of the dihedral angle

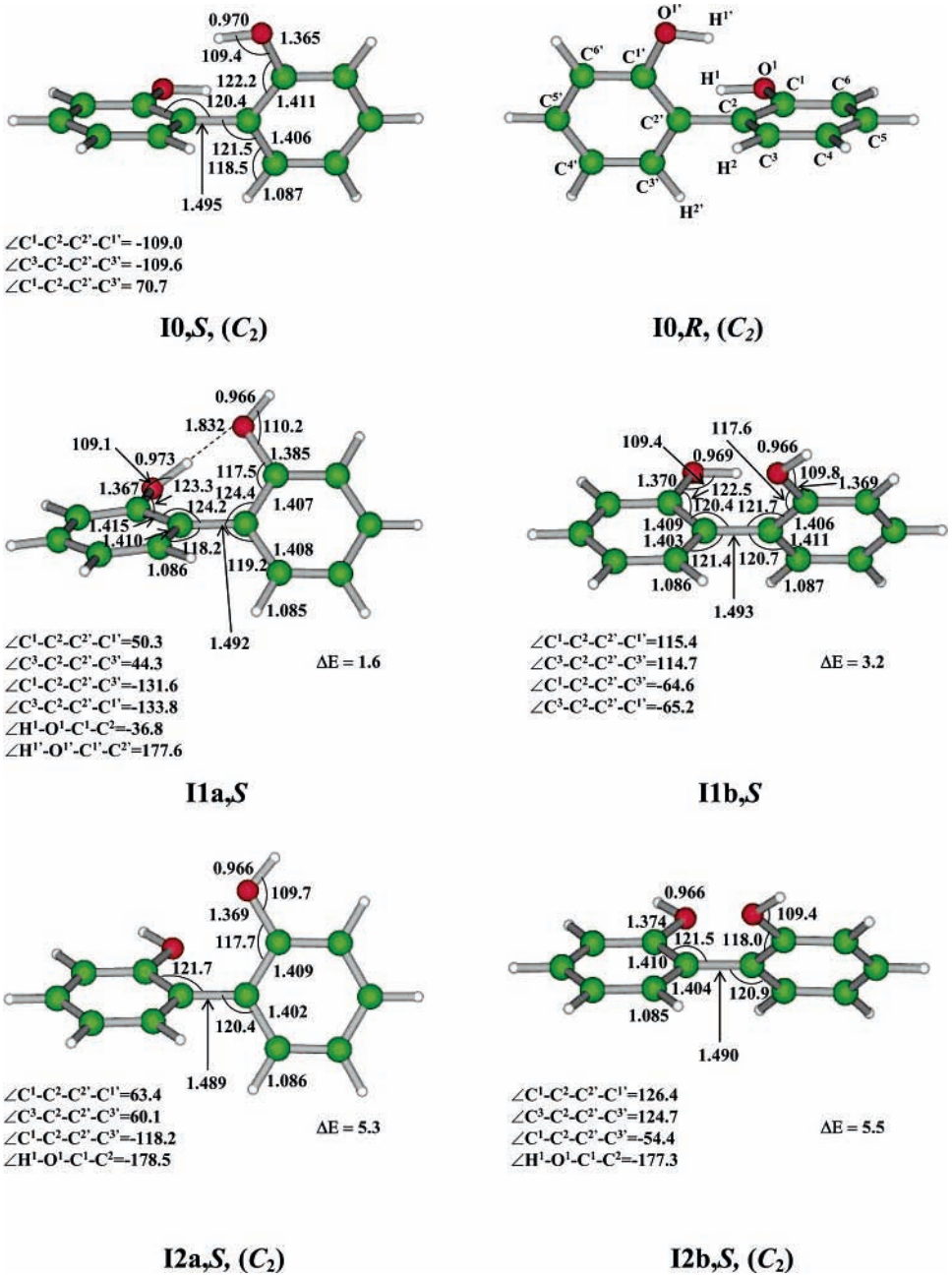

Figure 2. Optimized geometrical structures of the five isomers of 2,2′-biphenol. Only the most important dihedral angles are given and those relative to the planarity of the system, which undergo small variation, are not shown. Energies (ΔE) are in kcal mol^{-1}, distances are in angstroms, and angles and dihedral angles are in degrees. The energies are evaluated relative to the most stable isomer **I0**. Numbering of the selected atoms, shown in the structure of **I0,*R*** which is the mirror image of **I0,*S***, is identical for all structures presented in this paper. The symbol in parentheses denotes the irreducible representation of the point group of the isomer.

is that the parallel configuration of the two hydrogen atoms of the two OH groups yields an electrostatic repulsion between them and hence leads to enlargement of the rotational angle. Such an effect is absent in **I2a** due to the opposite directions of the two hydrogen atoms of the hydroxy groups. Another explanation that has been proposed for the case of **I0** ascribes the widening of the rotational dihedral angle to the electronic effect originating from the internal OH$\cdots\pi$ hydrogen bonds.[12,35] This suggestion was argued by the fact that a perpendicular arrangement between OH and the π of the corresponding aromatic ring favor the OH$\cdots\pi$ orbitals overlap. While this explanation is plausible for **I0** and seems to be applicable even for the binaphthol case (where the two aromatic rings are perpendicular to each other),[24] it is not the main factor governing their stabilities for the following two reasons. (i) The steric effect in binaphthol of the two aromatic rings brings the structure to a perpendicular arrangement between them. (ii) As will be shown later, in **I1a**−**I1b** isomerization, a perpendicular arrangement of one of the two OH groups with the π of its adjacent aromatic ring corresponds to a transition state structure. Looking at the values of the rotational dihedral angle in **I0**, **I1b**, and **I2b** (range from 109.6° to 126.4°), one can conclude that the electrostatic effect is the dominant factor in their structures.

3b. S−R Enantiomerization between the Most Stable Enantiomers. Consider the enantiomerization between the most stable enantiomers **I0,*S*** and **I0,*R***. Generally, there are two possible pathways for each enantiomerization process, trans and cis paths, depending on the rotational direction around the C−C single bond connecting the two aromatic rings. Here, in the trans path, the two OH groups get away from each other, while in

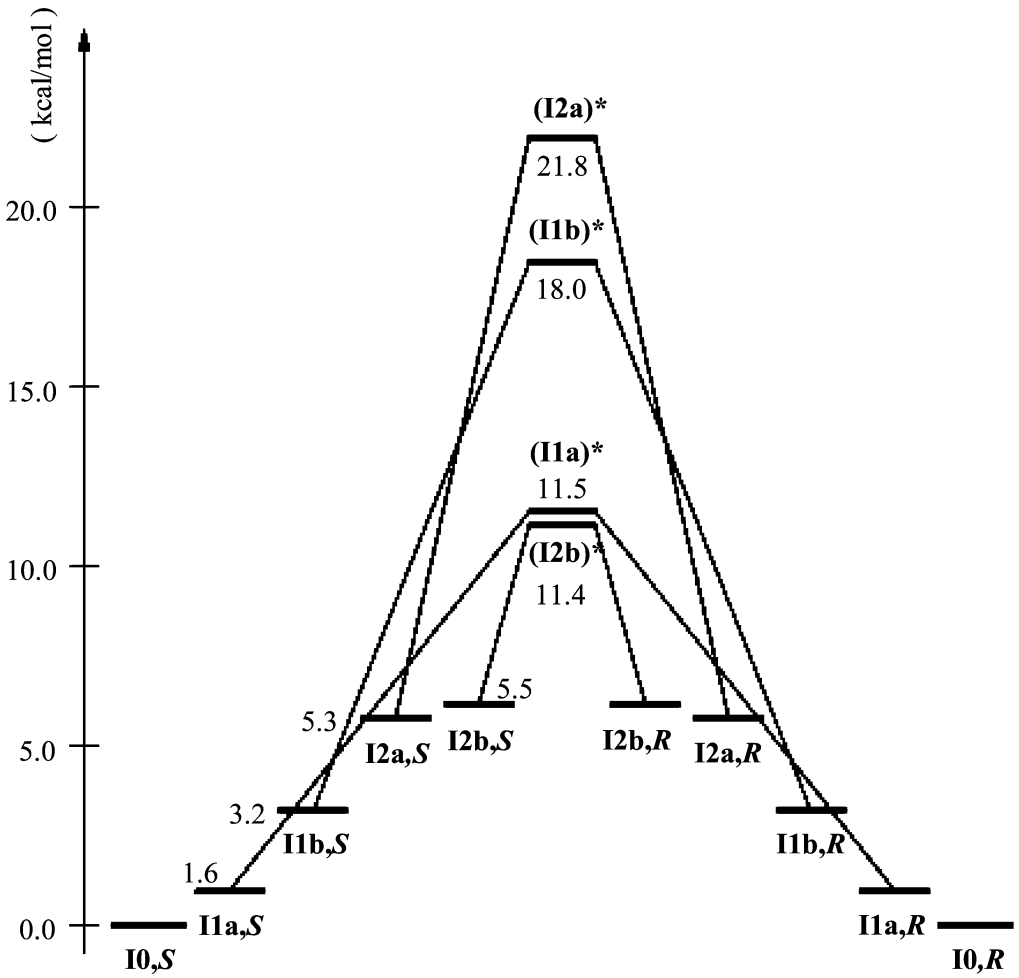

Figure 3. Energy diagram for direct enantiomerizations. There exists no direct enantiomerization process between **I0,*S*** and **I0,*R***. Names superscripted with an asterisk, (**I1a**)*****, and so forth, denote transition states of the other direct enantiomerizations. The numerical values are barrier heights of relevant enantiomers or transition states, which are measured from the most stable isomer **I0**. Its absolute energy is −613.792959 au.

the cis path the two OH groups get closer. In both paths, a rotation of 180° is considered.

The direct enantiomerization between **I0,*S*** and **I0,*R*** has no transition state along both the cis and the trans paths from the results of transition state searching by using an ab initio MO method, and this process is forbidden. Here, "direct" means enantiomerization through phenyl-ring rotation while OH rotation is frozen. Actually, in the course of the location of the transition state through C−C inter-ring bond rotation, none has been found connecting **I0** to any of the other isomers, regardless of whether the symmetry has been constrained or released. The main reason for the forbidden process is that there exists a strong electrostatic interaction between the two OH groups in the case of the cis path and a steric hindrance between H^2 and $H^{2'}$ in the case of the trans path.

Therefore, we take into account another enantiomerization process between the most stable enantiomers, which involves isomerization and direct enantiomerizations as the intermediate processes.

We first consider the other four direct enantiomerization processes **I1a,*S*−I1a,*R***, **I1b,*S*−I1b,*R***, **I2a,*S*−I2a,*R***, and **I2b,*S*−I2b,*R*** as the intermediate processes of enantiomerization **I0,*S*−I0,*R***. The enantiomerization processes **I1a,*S*−I1a,*R*** and **I2a,*S*−I2a,*R*** proceed via cis paths while **I1b,*S*−I1b,*R*** and **I2b,*S*−I2b,*R*** proceed via trans paths. We second consider isomerization processes as an intermediate process, and finally we examine the most probable enantiomerization pathways involving isomerization and direct enantiomerization processes.

(i) Direct S−R Enantiomerizations. Figure 3 shows the energy diagram for direct enantiomerizations, while Figure 4 shows the transition state structures. In general, any transition state for enantiomerization is characterized by an achiral structure. The numerical values in parentheses show imaginary vibrational frequencies that were calculated at the B3LYP/6-31+G(d,p) level.

*S−R Enantiomerization of **I1a**.* Direct enantiomerization takes place via transition state (**I1a**)***** along the cis-type of rotation of phenol rings. The two aromatic rings in the transition state are coplanar, forming a C_s symmetry. The main structural feature in the transition state (**I1a**)***** is the formation of an intramolecular hydrogen bond between the hydrogen atom of one hydroxy group and the oxygen atom of the other hydroxy group. Figure 4 shows the structure of (**I1a**)***** together with selected geometrical parameters. As a consequence of the hydrogen bonding, the $O^1C^1C^2$ angle increases by about 4° and that of $H^1O^1C^1$ increases by about 3°, compared to their respective angles in **I1a,*S***. The hydrogen bond also stabilizes the transition state, compared with those in the other transition state (see Figure 4), which is reflected in the height of the energy barrier (9.9 kcal mol^{-1} with respect to the energy of **I1a**).

*S−R Enantiomerization of **I1b**.* This enantiomerization takes place via the trans path. The transition state (**I1b**)***** connecting **I1b,*S*** and **I1b,*R*** enantiomers has a C_i symmetry, where the two OH groups are oriented in opposite directions but toward the aromatic rings counterpart, as shown in Figure 4. The dihedral angle formed by the two rings ($C^{1'}C^{2'}C^2C^1$) is 180°. However,

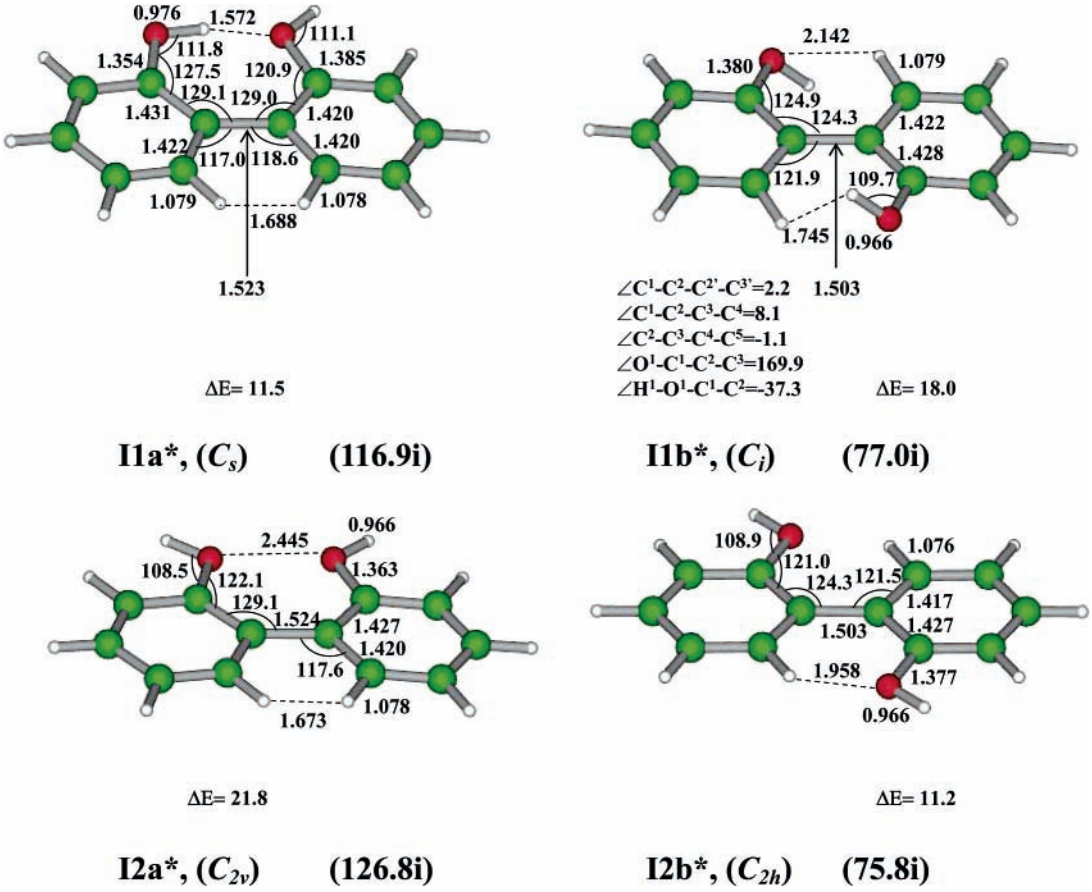

Figure 4. Transition state structures related to direct enantiomerizations. The values in parentheses indicate imaginary vibrational frequencies. ΔE is evaluated relative to **I0** and expressed in kcal mol^{-1}.

a nonnegligible out-of-plane deformation of the planarity of both rings has been identified, where the out-of-plane dihedral angle ($C^1C^2C^3C^4$) was estimated to be 8.1°. Similarly, both oxygen atoms bend out-of-plane of their aromatic rings by 10.1°. Both hydrogen atoms of the two hydroxy groups were found to point toward the aromatic ring counterpart by an angle of 37.3°. Moreover, the steric hindrance originating from the somehow short distance between the hydrogen atom of the OH group and its corresponding one of the aromatic ring counterpart, 1.745 Å, dominates the intramolecular hydrogen bond effects between the two rings, as deduced from its distance of 2.142 Å. This has its consequences on the stability of the transition state by raising the energy barrier up to 14.8 kcal mol^{-1} with respect to the energy of **I1b**.

S−*R Enantiomerization of **I2a**.* The process of the enantiomerization between **I2a,*S*** and **I2a,*R*** is similar to that in cis enantiomerization between **I1a,*S*** and **I1a,*R***. The structural features of the transition state (**I2a**)***** in the cis process are similar to that of (**I1a**)*****, with the exception of the opposite orientation of the two OH groups, as shown in Figure 4. This transition state has C_{2v} symmetry. The strong electrostatic repulsion between the two oxygen atoms, which are coplanar to the plane of the molecule, yields openings in $O^1C^1C^2$ and $O^{1'}C^{1'}C^{2'}$, designated OCC, and $C^1C^2C^{2'}$ and $C^{1'}C^{2'}C^2$, designated CCC, bond angles by 4.4° and 7.4°, respectively, compared with those in **I2a**. On the other hand, a second electrostatic repulsion takes place between H^2 and $H^{2'}$ as a result of narrowing of the CCC inter-ring bond angles to which they are attached ($C^3C^2C^{2'}$ and $C^{3'}C^{2'}C^2$). These two electrostatic effects enhance the energy barrier to 16.5 kcal mol^{-1} with respect to the energy of **I2a**. Hydrogen bond characterizing (**I1a**)***** is absent in the structure of (**I2a**)***** and significantly raises the height of the energy barrier, compared to the cis-enantiomerization for **I1a**.

S−*R Enantiomerization of **I2b**.* The transition state (**I2b**)* connecting **I2b,*S*** and **I2b,*R*** located along trans rotation of the phenol groups has a C_{2h} symmetry, in which the two OH groups are coplanar with the plane of the molecule, as can easily be seen from its structure depicted in Figure 4. The distance between the oxygen and hydrogen atoms of the other aromatic ring $O^1\cdots H^2$ is of the order of 1.958 Å, which is in the limit of the hydrogen bonding. Such weak interaction contributes to the stabilization of the transition state (**I2b**)***** and hence reduces the height of the energy barrier of the enantiomerization. Despite the two hydrogen bonds formed in the molecule, there is an enlargement of the bond angles OCC ($O^1C^1C^2$ and $O^{1'}C^{1'}C^{2'}$) and inter-ring bond angles CCC ($C^1C^2C^{2'}$ and $C^{1'}C^{2'}C^2$) compared to those in the structure of **I2b**. For OCC, the enlargement was 3.0°, while that for the CCC inter-ring bond angle was 2.8°. This result is attributed to a slight steric hindrance between the two aromatic rings, more precisely between C^1 and $C^{2'}$ on one hand and C^2 and $C^{1'}$ on the other hand. The calculated energy barrier for (**I2b**)***** is 5.9 kcal mol^{-1} with respect to the energy of **I2b**, the lowest energy barrier among all of the enantiomerization pathways. This value clearly indicates that the two hydrogen bonds greatly contribute to the stabilization of the transition sate (**I2b**)*.

(ii) Isomerizations. Figure 5 shows the energy diagram of isomerizations of *S*-enantiomers. The energy diagram of *R*-enantiomers was omitted because it is a mirror image of that of *S*-enantiomers.

(a) Isomerizations via OH rotation. The transition state structures appearing in the isomerization processes are shown

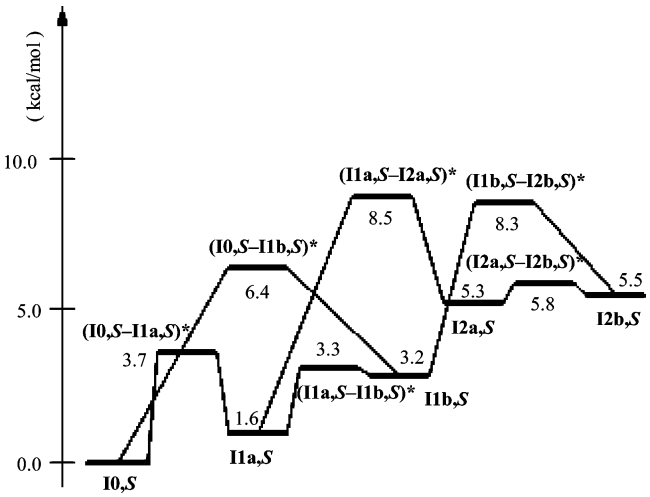

Figure 5. Energy diagram for the isomerizations of *S*-enantiomers.

in Figure 6. Numbers in parentheses show the imaginary vibrational frequencies that were calculated at the B3LYP/6-31+G(d,p) level.

First, consider the isomerization obtained by rotation of the OH groups. The transition states are (**I0,*S*−I1a,*S***)*, which connects **I0** to **I1a,*S***, or (**I0,*S*−I1b,*S***)*, which connects **I0** to **I1b,*S***, depending on the direction of the rotation, clockwise or counterclockwise.

The transition state (**I0,*S*−I1a,*S***)* reduces the height of the energy barrier compared to that of (**I0,*S*−I1b,*S***)* by about 2.7 kcal mol^{-1}. There are two possible reasons for the reduction of the energy. One is an intramolecular hydrogen bonding which is present in (**I0,*S*−I1a,*S***)* structure, while no such OH-bonding exists in (**I0,*S*−I1b,*S***)* one (see Figure 6). The other reason is electrostatic repulsion between the two hydrogen atoms of the two hydroxy groups in (**I0,*S*−I1b,*S***)*, which widens the ring−ring dihedral angle by about 71° compared to that in (**I0,*S*−I1a,*S***)*.

Similarly, consideration of rotation of the OH groups yields the location of the transition state (**I1a,*S*−I2a,*S***)* that connects **I1a** to **I2a** or (**I1b,*S*−I2b,*S***)* that connects **I1b** to **I2b**, depending on the direction of the rotation—clockwise or counterclockwise. The structures of all transition states resulting from OH rotations as well as their respective relative energies are presented in Figure 6. Because of triviality, the respective mirror images of the transition states are not shown. In all structures, the most significant feature is the orientation of the OH groups with respect to the plane of the aromatic rings.

For **I1a,*S*−I2a,*S*** or **I1b,*S*−I2b,*S*** isomerizations, the transition states (**I1a,*S*−I2a,*S***)* and (**I1b,*S*−I2b,*S***)* have similar energy barriers (8.5 and 8.3 kcal mol^{-1}, respectively). No intramolecular OH-bond exists in either structure. The enhancement in the energy barrier in (**I1a,*S*−I2a,*S***)* compared to that in (**I0,*S*−I1a,*S***)* comes from the energy required for the

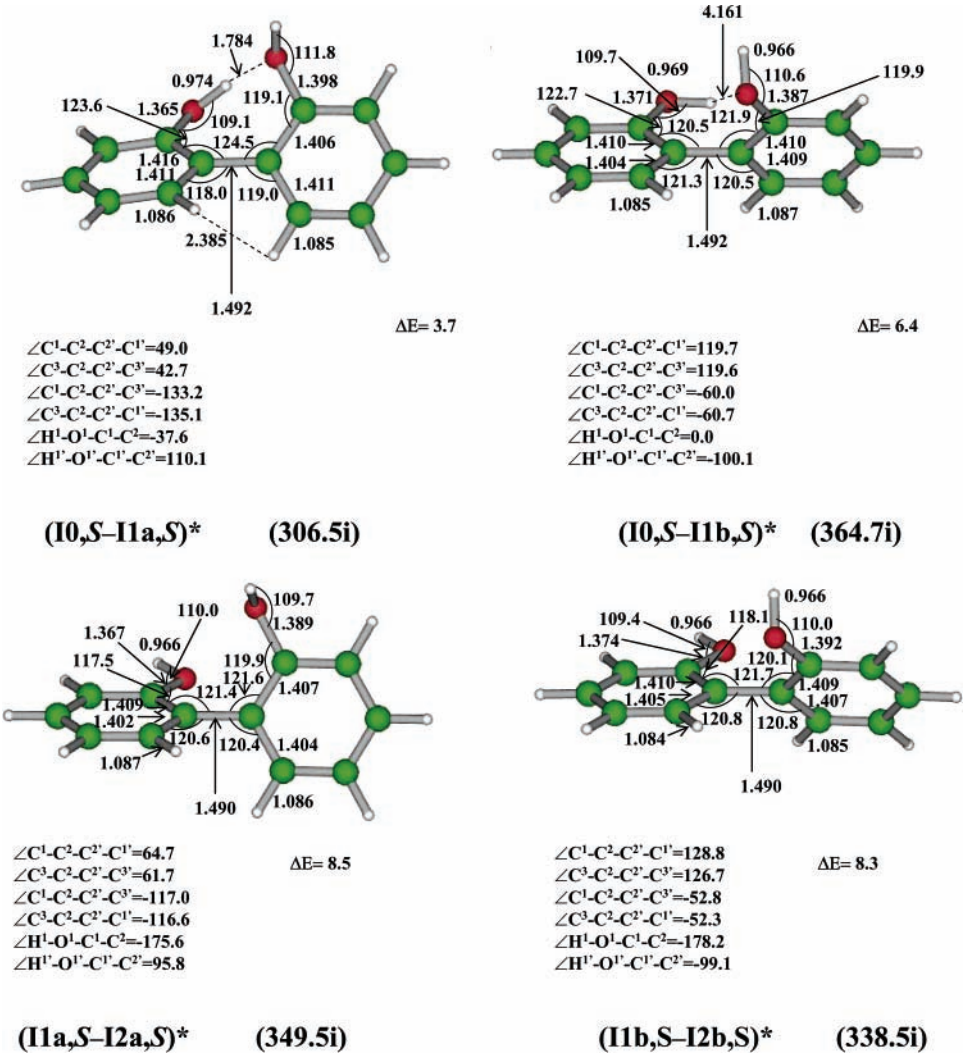

Figure 6. Transition state structures related to isomerization processes through OH-rotation. The values in parentheses indicate imaginary vibrational frequencies. Δ*E* is evaluated relative to **I0** and is expressed in kcal mol^{-1}.

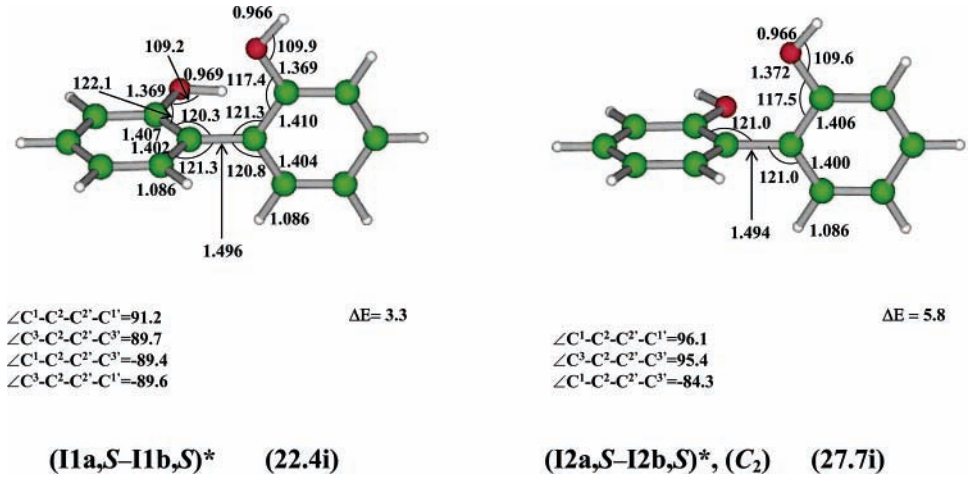

Figure 7. Transition state structures for the isomerizations of **I1a**−**I1b** and **I2a**−**I2b**. The values in parentheses indicate imaginary vibrational frequencies. ΔE is evaluated relative to **I0** and expressed in kcal mol^{-1}.

disruption of the OH-bond that exists in isomer **I1a**. The effects of steric hindrance and electrostatic repulsion on its stability are minor.

*(b) **I1a**−**I1b** and **I2a**−**I2b** Isomerizations.* Isomerizations **I1a**−**I1b** and **I2a**−**I2b** in which pairs of isomers have similar orientation of the two OH groups but different inter-ring bond angles take place easily via simple rotation around the C−C inter-ring bond connecting the two aromatic rings. The energy barrier for **I1a**−**I1b** isomerization is 1.7 kcal mol^{-1} (with respect to the energy of **I1a**), while that for **I2a**−**I2b** is 0.5 kcal mol^{-1} (with respect to the energy of **I2a**). Disruption of the OH···H bond in the course of **I1a**−**I1b** isomerization is the main factor that slightly enhances the height of the energy barrier compared to that in **I2a**−**I2b** isomerization. Except for the orientation of the two OH groups, the structures of the two transition states (**I1a**−**I1b**)* and (**I2a**−**I2b**)* exhibit similar geometrical features, particularly the perpendicular arrangement of the two aromatic rings, as shown in Figure 7. These low energy barriers indicate that isomers **I1b**, **I2a**, and **I2b** are difficult to isolate.

(iii) Enantiomerization Pathways between the Most Stable Enantiomers. In the previous section, we have evaluated single paths for enantiomerization and isomerization of biphenol. We now consider the enantiomerization paths of the most stable enantiomers. We restrict ourselves to a minimum number of transition states with less activation energies since optical transitions of the least number is preferable in quantum control. The most possible pathway is **I0,*S*** → **I1a,*S*** → **I1a,*R*** → **I0,*R***.

For comparative purposes, single-point energy calculations at the optimized B3LYP/6-31+G(d,p) structures have been carried out at the MP2(fc) using the same basis set. The results are summarized in Table 1. MP2 calculations nicely reproduce the energy trends obtained by B3LYP calculations. The high energy barrier obtained for (**I1a**)*, 17.0 kcal mol^{-1} (MP2) compared to 11.5 kcal mol^{-1} (B3LYP), may be attributed to the fact that the B3LYP structure is somehow away from the MP2 one, and therefore further optimization is needed. However, MP2 calculation is cost-ineffective; in addition, performance of frequency calculation at MP2 is computationally excessive and therefore we did not proceed with the calculation.

It should, however, be more interesting to take into consideration the thermochemical effects and to compare the trends to those obtained at the absolute temperature and pressure. To this end, we evaluated the zero-point energy correction (ZPE), the enthalpies (ΔH), entropies ($T\Delta S$), and Gibbs free energy (ΔG) with a scale factor of 0.9614[30] for calculated vibrational frequencies at the temperature of 298.15 K. As one can deduce from Table 1, the deviation is marginal between the results obtained for the enthalpies, entropies, and Gibbs free energy. Even the zero-point energy correction gave values very similar to those obtained with no correction. These results also show that the effect of the entropy in the enantiomerization pathway is negligible.

TABLE 1: Calculated Zero-Point Energy (ZPE), Potential Energies (ΔE), Enthalpies (ΔH), Entropies ($T\Delta S$), and Gibbs Free Energies (ΔG) Relative to I0 in kcal mol^{-1} for the Equilibrium Structures and Transition States of the Most Possible Enantiomerization Pathway: I0,*S* → I1a,*S* → I1a,*R* → I0,*R*

stationary point	relative energy[b]	ZPE[a]	ΔE^a	ΔH^a	ΔG^a	$T\Delta S^a$	$\nu_i{}^a$
I0	0.0	(***0.0***)[c]	0.0	0.0	0.0	0.0	0.0	
I1a	1.6	(***1.8***)[c]	1.7	1.6	1.6	2.0	−0.4	
(**I1a**)*	11.5	(***17.0***)[c]	11.3	10.9	10.9	11.5	−0.6	115.4 *i*
(**I0,*S*−I1a,*S***)*	3.7	(***3.9***)[c]	3.3	2.9	2.9	3.6	−0.7	307.6 *i*

[a] ΔH, $T\Delta S$, and $\Delta G = \Delta H - T\Delta S$ were calculated at $T = 298.15$ K. [b] Relative energy calculated with respect to the energy of the optimized structure of **I0** (−613.792959 au) without any correction. [c] In bold italic are results of MP2/6-31+G(d,p) single-point energy calculations at the B3LYP/6-31+G(d,p) optimized structures; the relative energy was calculated with respect to the MP2/6-31+G(d,p) energy of the structure of **I0** (−611.970904 au).

For quantum control in the above scheme, a sequence of pump−dump pulses can be applied to the enantiomerization in the electronic ground state. These pulses consist of IR ones. The first sequence pump−dump pulses are applied for creation of **I1a,*S*** from **I0,*S***, and then the second sequence pump−dump pulses are applied for obtaining the final product **I0,*R***.[38,39]

Finally, a comparison of the potential energy diagram of biphenol with that of binaphthol shows that attachment of a second aromatic ring to each of the first aromatic ones in biphenol drastically enhances the energy barrier.[24] The heights of the energy barriers in the biphenol enantiomerization/isomerization pathways are much smaller than those in binaphthol, with the exception of those involved in the OH-bond rotation pathways, which were found to be comparable. The energy limit of the most favorable path for biphenol is 11.5 kcal mol^{-1}, while that for binaphthol is 42.7 kcal mol^{-1}. This means that its quantum control for binaphthol using IR pulses is not possible but that quantum control via an electronic excited state is possible. On the other hand, quantum control of enantiomerization of biphenol in the electronic ground state is possible using IR.

4. Conclusion

The enantiomerization path for 2,2′-biphenol was theoretically investigated using the DFT (B3LYP) method. It was shown that the enantiomerization of the most stable isomer **I0** proceeds through intermediate processes, isomerizations, and direct enantiomerizations of other isomer pairs. The minimum energy required for the enantiomerization of **I0** was estimated to be 11.5 kcal mol^{-1}. The most possible enantiomerization path for quantum control of isomer **I0** is a sequence of pump and dump processes. In this case, the isomerization and direct enantiomerization involve the process of the least number of isomers. The isomerization through one of the two OH rotation paths is less energetic than that involving ring−ring rotation. The minimum energy required for the rotation of the two OH groups was estimated to be 8.3 kcal mol^{-1}.

Acknowledgment. R.S. acknowledges the receipt of a JSPS grant (P02353). Financial support from a grant-in-aid for Scientific Research (No. 14077215 and No. 17350004) from the Ministry of Education, Science, Sports, and Culture (to S.K. and Y.F.) is acknowledged.

References and Notes

(1) Dalterio, R. A.; Hurtubise, R. J. *Anal. Chem.* **1982**, *54*, 224−228.
(2) Saffioti, W.; Bueno, W. A. *J. Chim. Phys.* **1976**, *73*, 731−737.
(3) Keil, T.; Brzezinski, B.; Zundel, G. *J. Phys. Chem.* **1992**, *96*, 4421−4426.
(4) Kothainayaki, S.; Swaminathan, M. *J. Photochem. Photobiol. A*: *Chem.* **1997**, *102*, 217−221.
(5) Matsukawa, S.; Mikami, K. *Enantiomer* **1996**, *1*, 69−73.
(6) Mikami, K.; Matsukawa, S. *Nature (London)* **1997**, *385*, 613−615.
(7) Yonetake, K.; Takahashi, A.; Masuko, T.; Murouchi, S.; Kobayashi, T. *Polymer* **1995**, *36*, 4061−4067.
(8) Paris, F.; Balaguer, P.; Térouanne, B.; Servant, N.; Lacoste, C.; Cravedi, J.-P.; Nicolas, J.-C.; Sultan, C. *Mol. Cell. Endocrinol.* **2002**, *193*, 43−49.
(9) Chen, H.; Eastmond, D. A. *Carcinogenesis* **1995**, *16*, 2301−2307.
(10) Schwartz, R. D.; Williams, A. L.; Hutchinson, D. B. *Appl. Environ. Microbiol.* **1980**, *39*, 702−708.
(11) Reetz, M. T.; Merk, C.; Mehler, G. *J. Chem. Soc., Chem. Commun.* **1998**, 2075−2076.
(12) Maciel, L. S.; Bueno, W. A. *Can. J. Anal. Sci. Spectrosc*. **1997**, *42*, 79−83.
(13) Chen, X.-M.; Luo, G.-B.; Tong, M.-L.; Zhou, Z.-Y. *Acta Crystallogr., Sect. C*: *Cryst. Struct. Commun*. **1996**, *52*, 1727−1729.
(14) Kranz, M.; Clark, T.; Schleyer, P. v. R. *J. Org. Chem.* **1993**, *58*, 3317−3325, and references therein.
(15) Shapiro, M.; Brumer, P. *J. Chem. Phys.* **1991**, *95*, 8658−8661.
(16) Cina, J. A.; Harris, R. A. *J. Chem. Phys*. **1994**, *10*, 2531−2536.
(17) Salam, A.; Meath, W. J. *J. Chem. Phys*. **1997**, *106*, 7865−7868.
(18) Assion, A.; Baumert, T.; Bergt, M.; Brixner, T.; Kiefer, B.; Seyfried, V.; Strehle, M.; Gerber, G. *Science* **1998**, *282*, 919−922.
(19) Levis, J. R.; Menkir, G. M.; Rabitz, H. *Science* **2001**, *292*, 709−713.
(20) Fujimura, Y.; González, L.; Hoki, K.; Manz, J.; Ohtsuki, Y. *Chem. Phys. Lett.* **1999**, *306*, 1−8.
(21) Shapiro, M.; Frishman, E.; Brumer, P. *Phys. Rev. Lett.* **2000**, *84*, 1669−1672.
(22) Hoki, K.; Ohtsuki, Y.; Fujimura, Y. *J. Chem. Phys*. **2001**, *114*, 1575−1581.
(23) Hoki, K.; González, L.; Fujimura, Y. *J. Chem. Phys*. **2002**, *116*, 8799−8802.
(24) Sahnoun, R.; Koseki, S.; Fujimura, Y. *J. Mol. Struct.* **2005**, *735*, 315−324.
(25) Umeda, H.; Takagi, M.; Yamada, S.; Koseki, S.; Fujimura, Y. *J. Am. Chem. Soc.* **2002**, *124*, 9265−9271.
(26) Hoki, K.; Koseki, S.; Matsushita, T.; Sahnoun, R.; Fujimura, Y. *J. Photochem. Photobiol. A*: *Chem.*, in press.
(27) Hoki, K.; Sahnoun, R.; Koseki, S.; Fujimura, Y. To be published.
(28) Becke, A. D. *J. Chem. Phys.* **1993**, *98*, 5648−5652.
(29) Fukui, K.; Kato, S.; Fujimoto, H. *J. Am. Chem. Soc.* **1975**, *97*, 1−7.
(30) Scott, A. P.; Radom, L. *J. Phys. Chem.* **1996**, *100*, 16502−16513.
(31) Møller, M.; Plesset, M. S. *Phys. Rev.* **1934**, *46*, 618−622.
(32) Frisch, M. J.; Trucks, G. W.; Schlegel, H. B.; Scuseria, G. E.; Robb, M. A.; Cheeseman, J. R.; Zakrzewski, V. G.; Montgomery, J. A., Jr.; Stratmann, R. E.; Burant, J. C.; Dapprich, S.; Millam, J. M.; Daniels, A. D.; Kudin, K. N.; Strain, M. C.; Farkas, O.; Tomasi, J.; Barone, V.; Cossi, M.; Cammi, R.; Mennucci, B.; Pomelli, C.; Adamo, C.; Clifford, S.; Ochterski, J.; Petersson, G. A.; Ayala, P. Y.; Cui, Q.; Morokuma, K.; Rega, N.; Salvador, P.; Dannenberg, J. J.; Malick, D. K.; Rabuck, A. D.; Raghavachari, K.; Foresman, J. B.; Cioslowski, J.; Ortiz, J. V.; Baboul, A. G.; Stefanov, B. B.; Liu, G.; Liashenko, A.; Piskorz, P.; Komaromi, I.; Gomperts, R.; Martin, R. L.; Fox, D. J.; Keith, T.; Al-Laham, M. A.; Peng, C. Y.; Nanayakkara, A.; Challacombe, M.; Gill, P. M. W.; Johnson, B.; Chen, W.; Wong, M. W.; Andres, J. L.; Gonzalez, C.; Head-Gordon, M.; Replogle, E. S.; Pople, J. A. *Gaussian 98*, Revision A.11.3; Gaussian, Inc.: Pittsburgh, PA, 2002.
(33) Frisch, M. J.; Trucks, G. W.; Schlegel, H. B.; Scuseria, G. E.; Robb, M. A.; Cheeseman, J. R.; Montgomery, J. A., Jr.; Vreven, T.; Kudin, K. N.; Burant, J. C.; Millam, J. M.; Iyengar, S. S.; Tomasi, J.; Barone, V.; Mennucci, B.; Cossi, M.; Scalmani, G.; Rega, N.; Petersson, G. A.; Nakatsuji, H.; Hada, M.; Ehara, M.; Toyota, K.; Fukuda, R.; Hasegawa, J.; Ishida, M.; Nakajima, T.; Honda, Y.; Kitao, O.; Nakai, H.; Klene, M.; Li, X.; Knox, J. E.; Hratchian, H. P.; Cross, J. B.; Adamo, C.; Jaramillo, J.; Gomperts, R.; Stratmann, R. E.; Yazyev, O.; Austin, A. J.; Cammi, R.; Pomelli, C.; Ochterski, J. W.; Ayala, P. Y.; Morokuma, K.; Voth, G. A.; Salvador, P.; Dannenberg, J. J.; Zakrzewski, V. G.; Dapprich, S.; Daniels, A. D.; Strain, M. C.; Farkas, O.; Malick, D. K.; Rabuck, A. D.; Raghavachari, K.; Foresman, J. B.; Ortiz, J. V.; Cui, Q.; Baboul, A. G.; Clifford, S.; Cioslowski, J.; Stefanov, B. B.; Liu, G.; Liashenko, A.; Piskorz, P.; Komaromi, I.; Martin, R. L.; Fox, D. J.; Keith, T.; Al-Laham, M. A.; Peng, C. Y.; Nanayakkara, A.; Challacombe, M.; Gill, P. M. W.; Johnson, B.; Chen, W.; Wong, M. W.; Gonzalez, C.; Pople, J. A. *Gaussian 03*, Revision B.04; Gaussian, Inc.: Pittsburgh, PA, 2003.
(34) Calculations at the MP2(fc)/6-31G++(d, p) level confirm the existence of the five isomers found at the actual B3LYP level.
(35) Ottaviani, P.; Maris, A.; Caminati, W. *J. Mol. Struct.* **2004**, *353*, 695−696.
(36) Lucarini, M.; Pedulli, G. F.; Valgimigli, L.; Amorati, R.; Minisci, F. *J. Org. Chem.* **2001**, *66*, 5456−5462.
(37) Byrne, J. J.; Chavant, P. Y.; Averbuch-Pouchot, M.-T.; Vallé, Y. *Acta Crystallogr., Sect. C*: *Cryst. Struct. Commun.* **1998**, *54*, 1154−1156.
(38) Tannor, D. J.; Rice, S. A. *Adv. Chem. Phys.* **1988**, *70*, 441−523.
(39) Hoki, K.; Ohtsuki, Y.; Kono, H.; Fujimura, Y. *J. Phys. Chem. A* **1999**, *72*, 2665−2671.